Process optimization and modeling of lead removal using maleate/PAN nanocomposite nanofibers: characterization, kinetics and isotherm studies

Maryam Khashij[a], Parviz Mohammadi[b,*], Mina Babei[c], Mohammad Mehralian[a], Nasrin Aghamohammadi[d]

[a]Student Research Committee, Environmental Science and Technology Research Center, Department of Environmental Health Engineering, School of Public Health, Shahid Sadoughi University of Medical Sciences, Yazd, Iran, Tel./Fax: (+98) 8338281992; emails: m.khashij@yahoo.com (M. Khashij), mohammadmehralian@yahoo.com (M. Mehralian)
[b]Research Center for Environmental Determinants of Health (RCEDH), Health Institute and Department of Environmental Health Engineering, School of Public Health, Kermanshah University of Medical Sciences, Kermanshah, Iran, Tel. +98-9183593814; Fax: (+98) 8338281992; emails: parviz8855@yahoo.com/pmohammadi@kums.ac.ir (P. Mohammadi)
[c]Department of Materials and Textile Engineering, College of Engineering, Razi University, Kermanshah, Iran, Tel./Fax: (+98) 8338281992; email: maryam2030@yahoo.com (M. Babei)
[d]Centre for Occupational and Environmental Health, Department of Social and Preventive Medicine, Faculty of Medicine, University of Malaya, 50603 Kuala Lumpur, Malaysia, Tel./Fax: (+98) 8342281932; email: nasrin@ummc.edu.my (N. Aghamohammadi)

ABSTRACT

This study aims to investigate the efficiency of lead (Pb) adsorption by adsorbent maleate/polyacrylonitrile nanocomposite using immersing the pristine electrospun (PAN) nanofibers. Characterizations such as field emission scanning electron microscopy, transmission electron microscopy, and Fourier transform infrared spectroscopy were applied to investigate the structure of the synthesized maleate nanoparticles. FESEM image indicates the smooth surface of the PAN nanofibers and the maleate nanoparticles coating on the electrospun PAN nanofibers surface. A four-factor central composite design was employed, with six replicas at the central points to optimize the process variables. The maximum Pb removal percentage of 98.5% was achieved at the initial concentration of 25 mg/L, an adsorbent dosage of 1.85 g/L, a pH of 6, and a contact time of 60 min. The adsorption process follows the Langmuir isotherm ($R^2 = 0.99$) and pseudo-second-order kinetics ($R^2 = 0.99$). The highest capacity of Pb ions adsorption through maleate/PAN nanocomposite was 349.15 mg/g that makes it a potential adsorbent in wastewater treatment.

Keywords: Adsorption; Electrospinning; Lead removal; Maleate nanoparticles; RSM

1. Introduction

Nowadays, one of the most important environmental problems throughout the world is the pollution of water resources due to the discharge of industrial wastewater containing heavy metals [1]. Heavy metals such as mercury, lead, cadmium, and arsenic, due to high toxicity can endanger human health even at trace concentrations [2]. Therefore, it should be removed from wastewater before being discharged into the receiving water because of their stability and non-biodegradability in nature [3]. Various treatment methods such as filtration, bioremediation, chemical oxidation, ion-exchange, and adsorption have been investigated for removal of these heavy metals from

* Corresponding author.

contaminated water [4]. Among these methods, the adsorption process due to simplicity, feasibility, recovery of metal, easy in operation, and versatility has been considered as an economical method for the removal of heavy metals [5]. Today, different adsorbents, such as zeolites, metal oxides, clays, and other materials have been used for the adsorption of heavy metals [6–9]. Maleate nanoparticles (reaction between carboxylic acids and iron oxy-hydroxides), among various types of nanoparticles, are promising candidates to efficiently adsorb pollutants in case of water treatment, because of unique physical and chemical properties [6]. In addition, the residual nanoparticle in aqueous solution has two main problems: difficult recovery and easy aggregation in aqueous solution. Consequently, in order to solve these problems, much attention has been given to the use of adsorbents by loading them on another solid media (e.g., polymer materials) to prevent them from being washed off [10]. Nanofiber material with high porosity, extensive surface ratio, significant adsorption capacity and small interfibrous pore size has been used as the most effective sorbent for the removal of heavy metals in recent years [11]. A study by Maleki et al. [12] claimed that functionalization of maleate nanoparticle with nanofiber, not only increases its large accessible surface area but also improves its heavy metal absorption. In the present study, maleate/PAN nanocomposite fibers were synthesized using immersing the pristine electrospun (PAN) nanofibers. Maleate nanoparticle was selected as a functionalizing agent because of its high heavy metal adsorption capacity. The reason for the use of PAN nanofibers for loading maleate nanoparticles is that it can improve the removal of heavy metals owing to its electron-donating nature. The nanoparticles were able to bind to the surface of the polymer because of the presence of carboxyl groups on the surface of the nanoparticles. To our knowledge, maleate nanoparticle have not been used for the preparation of maleate/PAN nanocomposite. Then, the efficiency of maleate/PAN nanocomposite was investigated for lead ions removal. RSM based on a central composite design (CCD) was used for studying the interaction between variables by synthesized nanocomposite. Therefore, the aim of this study was designed to develop a novel nanocomposite for lead removal from aqueous solutions. Investigated experimental variables consist of maleate/PAN nanocomposite dosage, initial Pb ions concentration, pH, and contact time. All the variables were simultaneously used for calculation of their relative effects. In addition, the prepared maleate/PAN nanocomposites were characterized in terms of their morphology, structure, shape, and their crystallinity using SEM, FTIR, and TEM techniques, respectively.

2. Experimental setup

2.1. Materials

The compounds used in this study are as follows:

N,N-dimethylformamide (DMF), iron(II) chloride tetrahydrate ($FeCl_2·4H_2O$), potassium hydroxide (KOH), hexamethylenetetramine ($C_6H_{12}N_4$), sodium nitrate (NaN_2), maleic anhydride ($C_4H_2O_3$) were purchased from Merck (Germany). In addition, for preparing the stock solution, lead(II) nitrate ($Pb·(NO_3)_2$) (Merck, Germany) was used.

Polyacrylonitrile powder (PAN) (MW = 80 kg/mol) made from Iran Poly acryl company (Isfahan, Mobarakeh) was supplied as the polymer for the synthesis of PAN nanofibers by electrospinning technique.

2.2. Preparation of maleate nanoparticles

First, lepidocrocite was synthesized via the reaction of 12 g $FeCl_2·4H_2O$, 1.68 g $C_6H_{12}N_4$, and 4.2 g $NaNO_2$ in 50, 20, and 20 mL distilled water, respectively. For this purpose, $FeCl_2·4H_2O$ and hexamethylenetetramine solutions were mixed on the stirrer; then titrated with NaN_2 solution at 30°C. Solutions are sonicated (SONREX Digitec DT52 H, Bandelin, Germany) for 1 h at a temperature of 55°C. The obtained mixture was centrifuged and dried at room temperature for 1 h. In the second step, maleic ferroxane was synthesized by the reaction of lepidocrocite and maleic anhydride. Briefly, 6 g lepidocrocite and 9.8 g maleic anhydride mixed in 200 mL deionized water and refluxed for 20 h at boiling point. The precipitate finally obtained after centrifugation by Universal 320R centrifuge (Hettich, Germany) and was washed with deionized water and dried in an oven at 80°C and then, crushed and sieved by using a mesh number 60 (approximately 0.25 mm).

2.3. Electrospun maleate/PAN nanocomposite fibers preparation

The electrospinning setup (PARS NANO RIS Co., Kermanshah) for this work is shown in Fig. 1, which consists of the cylindrical collector, a high power source, nozzle, and syringe for the polymer injection. In electrospinning, the polymer solution through the syringe nozzle is poured into a grounded collector in the presence of the electrical field. Charging the polymer droplet leads to changes in its shape resulting in a Taylor cone. On the other hand, increasing the electrical power causes excessive electrical forces from the droplet surface tension. During the jet of polymer to the collector, jet undergoes bending instability due to the charge repulsion on its surface which causes in the formation of very long fibers. Finally, with the evaporation of the solvent, the polymeric fibers on the grounded collector are deposited. The conditions for PAN electrospinning were obtained as follows: the temperature of 23°C, relative humidity of 20%, the voltage of 22 kV, and 9 cm gap between nozzle and collector. For PAN nanofibers preparation, an aqueous solution of PAN was made based on Moradi et al. [5], by mixing 1.5 g PAN (Mw = 80 kg mol^{-1}) and 10 g DMF (99.8%) for 16–24 h at 60°C until homogeneous solutions are achieved for electrospinning application. The synthesized solution was loaded in a plastic syringe with a blunt stainless steel needle (0.31 mm internal diameter) and fed constantly by a syringe pump at 1 mL/h. Electrospun fibers were obtained by applying a voltage of 22 kV with a high voltage DC power supply. Surface collector with an indium tin oxide conductive and glass fabric coating was used to collect the fibers. In order to coat maleate nanoparticles to nanofiber mat, appropriate amount of nanoparticles was dispersed into a 50 mL acetone solution (Chemical Grade, Nashik, Maharashtra). The solution obtained was poured slowly and uniformly on the nanofibers mat.
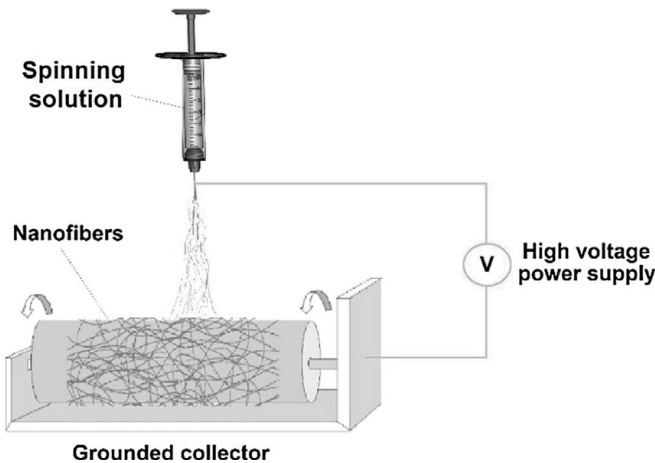
Fig. 1. Electrospinning setup (PARS NANO RIS Co.).

2.4. Adsorbent characterization

Lepidocrocite and maleate nanoparticles were characterized by Fourier-transform infrared (FTIR) and SEM analyses. FTIR analysis was done in the range of 400 and 4,000 cm^{-1} with KBr pellets at 25°C (Bruker alpha, Germany). To observe the surface morphology of nanoparticles and membrane adsorbents, scanning electron microscopy (SEM, Philips XL-30S FEG and LEQ1450 VP, Netherlands) was used. Transmission electron microscopy (TEM) image of maleate/PAN nanocomposite fibers was recorded by Philips CM120 (Netherlands).

2.5. Experimental design based on CCD

The statistical techniques are combined in RSM to optimize the processes and evaluate the significance of various parameters [13]. The experimental design technique is applied to recognize the performance of adsorption process. Applying RSM leads to achievable minimum experimental runs and subsequently reduces the materials consumption [14]. RSM was applied for evaluation of the independent variables such as initial lead concentration (A), maleate/PAN dose (B), pH (C), and contact time (D) on the adsorption process. The experimental runs on conditions of variables, based on CCD, are shown in Table 1.

The lead removal percentage (Y) was served as a response. Experimental analysis including regression analysis and analysis of variance (ANOVA) was done by Design-Expert version 7.00. The regression model based on the quadratic equation (Eq. (1)) was performed to anticipate the optimum condition and interaction between independent variables.

$$R = \alpha_0 + \sum_{i=1}^{k} \alpha_i x_i + \sum_{i=1}^{k} \alpha_{ii} x_i^2 + \sum_{i=1}^{k-1} \sum_{j=i+1}^{k} \alpha_{ij} x_i x_j + \varepsilon \qquad (1)$$

where R: the response; k: the number of parameters; x_i and x_j: selected parameters; α_0, α_i, α_{ii} and α_{ij}: constant, linear, quadratic and second-order interaction coefficients, respectively, and ε: the experimental error of parameters. The fit quality of quadratic model was explained by descriptive statistics such as determination coefficient (R^2), F-value,

p-value, the degree of freedom (DF), the coefficient of variation (C.V.), and the sum of squares (SS).

2.6. Adsorption process experiments

The batch adsorption process experiment was conducted by treating the prepared stock solutions with different ranges of maleate/PAN nanocomposite dosage from 0.7 to 3 g/L, with varying agitation time from 30 to 90 min, pH of adsorption process from 4 to 6 based on the design obtained from the CCD arrangement. In order to provide the required initial solution of Pb solution, lead stock (1,000 mg/L) was diluted with distilled water. The pH was adjusted using HCl (1 M) and NaOH (1 M) and controlled by pH meter (HQ40d). Appropriate amounts of adsorbent and 50 mL of their queried concentration of Pb(NO$_3$)$_2$ solutions were placed in a 100 mL Erlenmeyer flask with a constant agitation rate of 180 rpm in a shaker at ambient temperature ranged from 25°C to 30°C. Finally, supernatants were analyzed using atomic absorption spectrophotometer PG-990 (PG 13 Instruments Limited, United Kingdom) to determine lead concentration. The heavy metal removal efficiency and amount of adsorption were calculated by Eqs. (2) and (3), respectively.

$$E = \frac{C_0 - C_e}{C_0} \times 100 \qquad (2)$$

$$q = (C_0 - C_e) \times \frac{V}{M} \qquad (3)$$

where E is the removal efficiency, C_0 (mg/L) and C_e (mg/L) are the initial and final Pb concentrations in the solution, respectively. q (mg/g) is adsorption capacity, V (L) is the solution volume, and M (g) is the amount of applied adsorbent.

For isotherms adsorption modeling, the results using linear forms of Langmuir, Freundlich, and Dubinin–Radushkevich (D-R) equations (Eqs. (4)–(8)) were analyzed as follows [15]:

$$\frac{C_e}{q_e} = \frac{1}{q_{max} K_L} + \frac{C_e}{q_{max}} \qquad (4)$$

$$\ln q_e = \frac{1}{n} \ln C_e + \ln K_f \qquad (5)$$

$$\ln q_e = -\beta \varepsilon^2 + \ln q_{m,D\text{-}R} \qquad (6)$$

$$\varepsilon = RT \ln \left(\frac{C_e + 1}{C_e} \right) \qquad (7)$$

$$E = \frac{1}{\sqrt{2\beta}} \qquad (8)$$

where q_e is the Pb equilibrium concentration (mg/g); q_{max} is the maximum adsorption (mg/g); K_L and K_f represent Langmuir (1/mg) and Freundlich (mg/g) constant, and n shows the adsorption rate. Parameter of $q_{m,D\text{-}R}$ (mg/g) is

Table 1
CCD and experimental values of Pb removal

Run	Pb concentration (mg/L)		Adsorbent dosage (g/L)		pH		Contact time (min)		Removal (%)
	Coded	Actual	Coded	Actual	Coded	Actual	Coded	Actual	
1	0	25	0	1.85	0	6	–1.5	15	85
2	–1	10	–1	0.7	–1	5.0	–1	30	40
3	–1	10	–1	0.7	1	7.0	–1	30	47
4	–1	10	1	3.0	–1	5.0	–1	30	52
5	–1	10	1	3.0	1	7.0	–1	30	55
6	1	40	–1	0.7	–1	5.0	–1	30	66
7	1	40	–1	0.7	1	7.0	–1	30	77
8	1	40	1	3.0	–1	5.0	–1	30	73
9	1	40	0	1.85	1	7.0	–1	30	78
10	0	25	0	1.85	0	6.0	0	60	98.5
11	0	25	0	1.85	0	6.0	0	60	97.9
12	0	25	0	1.85	0	6.0	0	60	97.5
13	0	25	0	1.85	0	6.0	0	60	90
14	0	25	0	1.85	0	6.0	0	60	98
15	0	25	0	1.85	0	6.0	0	60	93
16	0	25	–1	0.7	0	6.0	0	60	67
17	0	25	0	1.85	0	6.0	0	60	58
18	1	40	0	1.85	0	6.0	0	60	83
19	0	25	0	1.85	–1	5.0	0	60	68
20	0	25	0	1.85	1	7.0	0	60	68
21	0	25	1	3.0	0	6.0	0	60	80
22	–1	10	–1	0.7	–1	5.0	1	90	43
23	–1	10	–1	0.7	1	7.0	1	90	53
24	–1	10	1	3.0	–1	5.0	1	90	65
25	–1	10	1	3.0	1	7.0	1	90	67
26	1	40	–1	0.7	–1	5.0	1	90	68
27	1	40	–1	0.7	1	7.0	1	90	76
28	1	40	1	3.0	–1	5.0	1	90	78
29	1	40	1	3.0	1	7.0	1	90	81
30	0	25	0	1.85	0	6.0	1.5	105	96

the theoretical maximum adsorption capacity of the D-R isotherm. β (mol²/kJ²) is the affinity coefficient regarding the free energy of adsorption process and ε constant is the Polanyi potential energy. R and T (K) are the universal gas constant and the absolute temperature, respectively. E (kJ/mol) is average adsorption free energy [15]. Besides, the equilibrium data using pseudo-first-order and pseudo-second-order kinetics were modeled. The correlation coefficient (R^2) was used for the correlation between experimental results and models.

The pseudo-first-order and pseudo-second-order kinetics are as follows [16]:

$$\log\left(q_e - q_t\right) = \log q_e - K_1 t \tag{9}$$

$$\frac{t}{q_t} = \frac{1}{K_2 q_e^2} + \frac{1}{q_e} \tag{10}$$

where q_t and q_e are the amount of Pb on the nanocomposite at time t and at equilibrium time (mg/g) respectively, and K_1 (1/min) and K_2 (mg/(g min)) represents the pseudo-first-order and pseudo-second-order constants. The $\log(q_e - q_t)$ vs. t graph for determination of R^2 coefficient and K rate and regarding obtaining the speed parameters, the t/q_t vs. t chart has been used. Based on the t/q_t vs. t graph and according to slope and y-intercept, the q_e and K_2 were calculated.

3. Results and discussion

3.1. Electrospun maleate/PAN nanocomposite nanofibers characterization

The surface morphology of electrospun maleate/PAN nanocomposite nanofibers was characterized by FESEM (Fig. 2). Fig. 2a confirmed the orientated PAN nanofibers with the average diameter of 209.6 ± 32.0 nm. As shown in
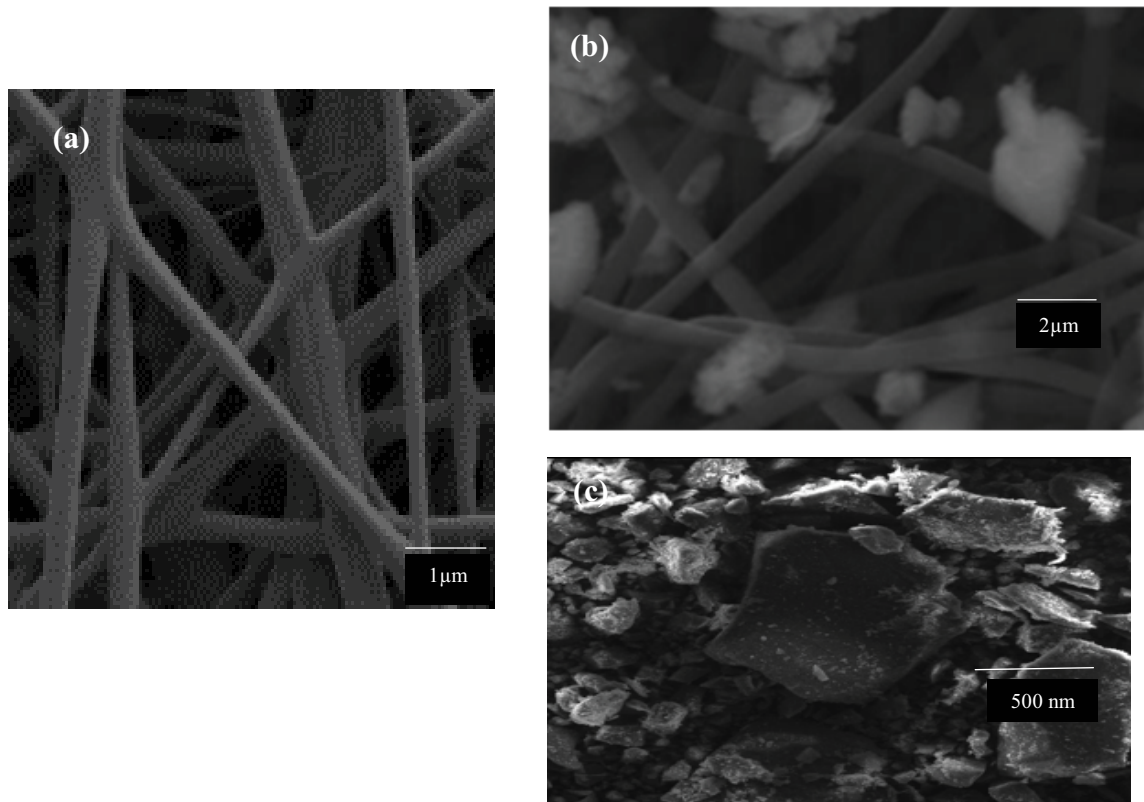
Fig. 2. FESEM graphs of electrospun: (a) PAN, (b) maleate/PAN nanofibers, and (c) TEM images of maleate nanoparticles.

Fig. 2b, the surface of the nanofibers was not smooth in electrospun maleate/PAN nanocomposite and maleate nanoparticles could be observed on the PAN nanofibers surface, which created a high adsorption capacity for Pb ions. The TEM images (Fig. 2c) of the surface in maleate/PAN nanocomposite nanofibers reveals that the maleate nanoparticles were loaded on the PAN nanofiber surface. Fig. 2b reveals the good dispersion of maleate nanoparticles on the surface of the PAN nanofibers. As shown in Fig. 2c, the particle size is lower than 100 nm, which presented the nanostructure of particles.

The FTIR spectra of maleate nanoparticles are clearly shown in Fig. 3. Accordingly, in Fig. 3, peaks at 1,489 and 1,543 cm^{-1} were related to the carboxylate bond between lepidocrocite and maleic anhydride. The peak of 1,421 cm^{-1} was proofed for carboxylate groups of maleate [17]. The bands at 3,580 and 3,670 cm^{-1} were associated with the free –OH stretching. Peaks in the region 1,090–990 cm^{-1} were related to the S=O stretch. The bands are found between 550 and 750 cm^{-1} due to the X–H stretch of hydrogen-bonded water and amides. Indeed, the large tendency of the particles to strongly attract one another comes from the existence of the maleate and hydroxyl functional groups present on their surface and thus producing huge agglomerates.

3.2. Statistical analysis and modeling

A four-factor CCD was employed, requiring 30 experimental runs (calculated based on Eq. (1)), which consist of six replicas at the central points to optimize the process variables. The levels of variables using CCD are shown in Table 1. The model for Pb removal percentage concerning coded variables is defined in Eq. (11):

$$\%R = +95.61 + 10.37A + 4.82B + 3.34C + 2.90D - 2.06AB - 1.56AD - 1.44BC + 1.44BD - 11.00A^2 - 9.70B^2 - 9.22C^2 - 2.11D^2 \quad (11)$$

The significance of the model by F and p-values was investigated and the results are listed in Table 2. In statistical analysis, p-values lower than 0.05 is significant; and the higher F-value represents that it is more significant in the model [18]. Based on Table 2, the effect of variables: initial Pb concentration, adsorbent dosage, pH, and contact time was significant ($p < 0.0001$). The effects of squared terms of all terms of A^2, B^2, C^2, and D^2 and the interaction between parameters (concentration–dosage, dosage–pH, and dosage–time) were significant. The coefficient of determination (R^2) indicates the variance of the dependent variable that is predictable from the independent variables [19]. The adjusted determination coefficient, adj R^2, was performed for comparison between the model with different numbers of predictors [20]. The value of R^2(adj) equals to 0.97, which indicates that the model for Pb removal explained is 97% of the total variance. In addition, a good relationship between the response (removal of Pb) and the independent variables is provided. On the other hand, the p-value is lower than 0.05, which represents significant parameters, while the p-value related to lack of fit with a value of 0.9481 is insignificant. Based on
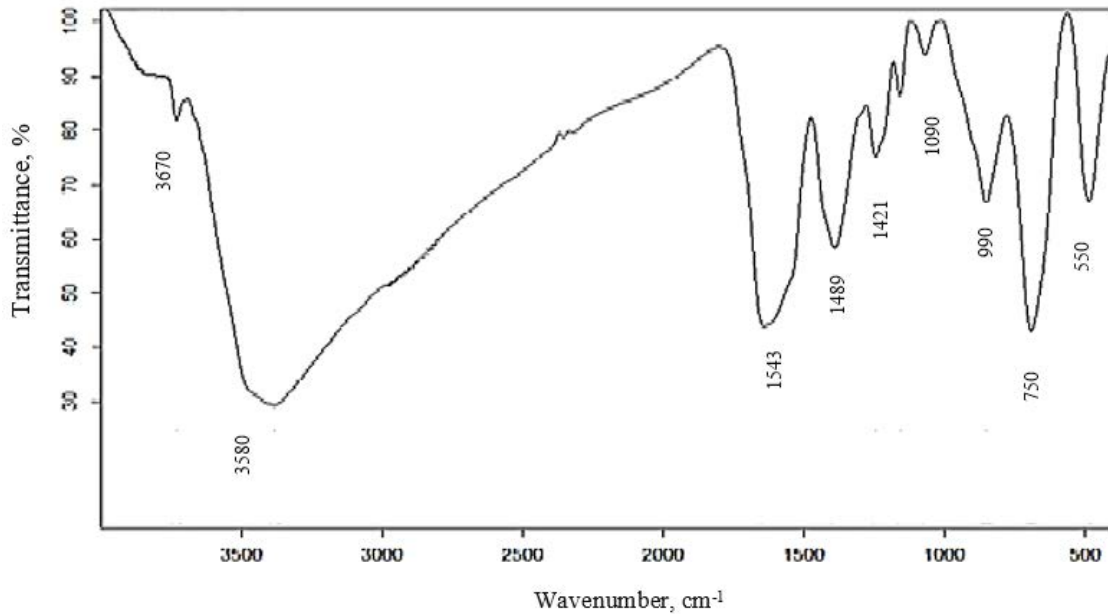
Fig. 3. FTIR spectra of the maleate nanoparticles.

Table 2
ANOVA results of the model of Pb removal using maleate/PAN nanofibers

Source model	Sum of squares	df	Mean square	F value	p-value Prob.>F
Model	8,376.94	12	698.08	108.81	<0.0001
A	2,202.74	1	2,202.74	343.35	<0.0001
B	475.11	1	475.11	74.06	<0.0001
C	228.89	1	228.89	35.68	<0.0001
D	172.70	1	172.70	26.92	<0.0001
AB	68.06	1	68.06	10.61	0.0046
AD	39.06	1	39.06	6.09	0.0245
BC	33.06	1	33.06	5.15	0.0365
BD	33.06	1	33.06	5.15	0.0365
A^2	1,376.05	1	1,376.05	214.49	<0.0001
B^2	1,065.69	1	1,065.69	166.11	<0.0001
C^2	967.16	1	967.16	150.75	<0.0001
D^2	50.63	1	50.63	7.89	0.0121
Residual	109.06	17	6.42		
Lack of fit	47.89	12	3.99	0.33	0.9481
Pure error	61.18	5	12.24		
Cor. total	8,486.00	29			
Adequate precision	34.23				
$R^2 = 0.98$	$R^2(adj) = 0.97$	$R^2(pred) = 0.96$			

p-value parameters regarding the fit model, Eq. (11) was statistically significant for Pb removal by maleate/PAN nanocomposite nanofibers in this study.

3.3. Effect of parameters on Pb removal

The model for Pb removal with electrospun maleate/ PAN nanocomposite as a function of the Pb concentration, dosage at different pH, and contact time is illustrated in Fig. 4. The Pb removal percentage depends on the dose of adsorbent concentrations and as the dosage increases around 2.5 g/L, the removal percentage increases. In fact, increasing the adsorbent dosage provides sufficient active sites for Pb ions adsorption using electrospun nanofibers nanocomposite. As shown in Fig. 4a, when the dosage of adsorbent increases to 2.5 g/L, it may increase the degree of unsaturation in the active sites, thus it leads to decreased availability of the active adsorption sites and the surface
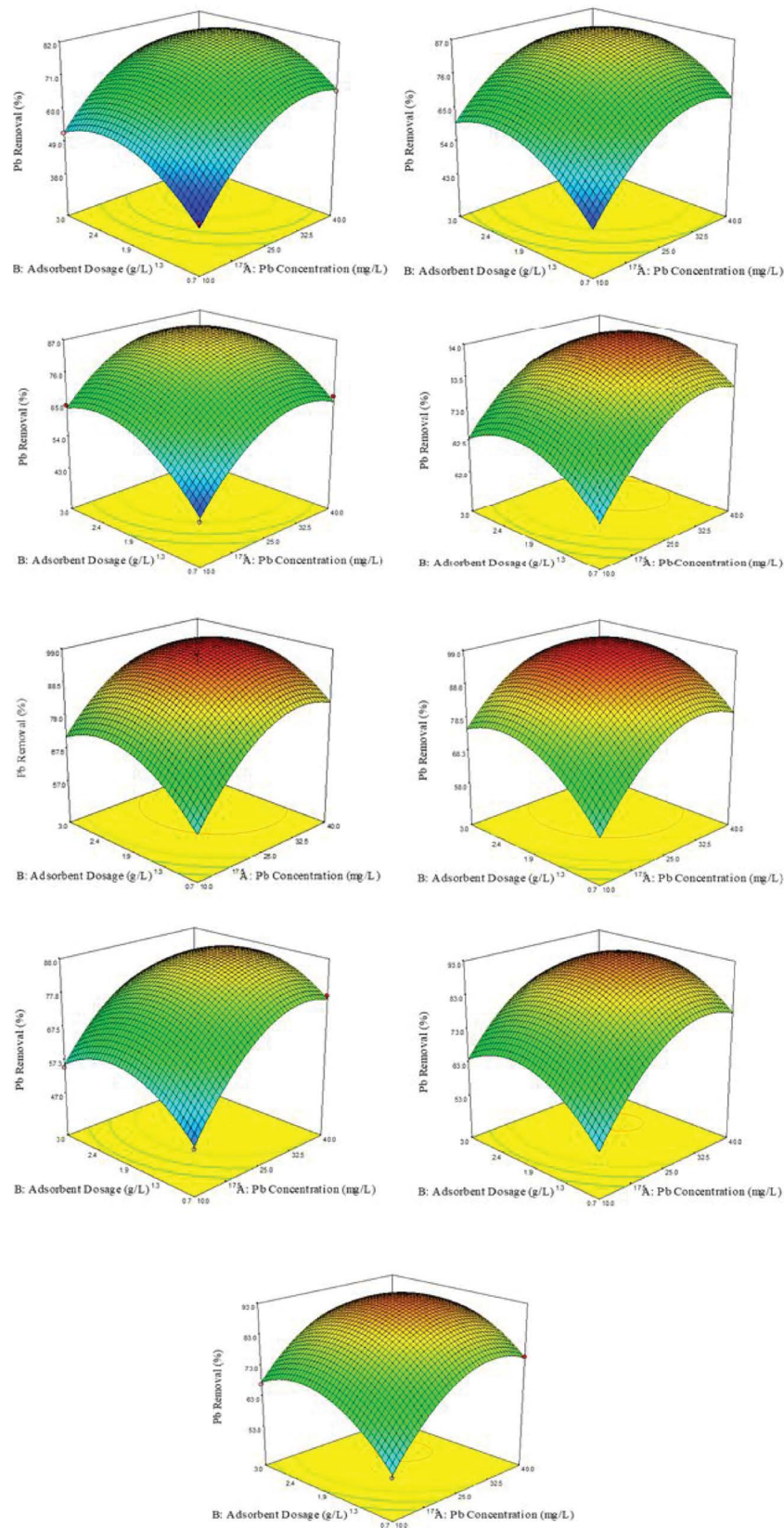
Fig. 4. Three-dimensional plots of the Pb concentration and dosage on the maleate/PAN nanocomposite efficiency at different pH and contact time. (a) 5 and 30 min, (b) 5 and 60 min, (c) 5 and 90 min, (d) 6 and 30 min, (e) 6 and 60 min, (f) 6 and 90 min, (g) 7 and 30 min, (h) 7 and 60 min, (i) 7 and 90 min and temperature 25°C.

area [21]. Indeed, it is clear that a further increase in adsorbent dosage (more than about 2.5 g/L) did not result in increasing Pb ions removal; because, although the active sites available on the adsorbent increase with increasing the nanofiber adsorbent dosage, these active sites remain unsaturated in adsorption process. The removal percentage of lead depends on the initial concentration of ions, as the concentration increases from approximately 10–34 mg/L the removal efficiency rapidly increases. This effect has been attributed to saturation of available active sites with high Pb concentration. Indeed, high concentration of heavy metal ions leads to occupation of adsorption sites and subsequent reduction of the number of active sites. Similar observations are agreed with the results. Based on Figs. 4a–i, when pH rises to around 6, the rate of Pb removal also increases at the same initial concentration and nanocomposite dosage, but increasing in pH nearly 7, Pb removal percentage decreased. On the other hand, however, contact time is not only an influential parameter for the lead adsorption particularly from 30 to 60 min but also the Pb removal rate was not substantially affected by increasing the contact time from 60 to 90 min. The Pb adsorption mechanism by maleate/PAN nanofibers indicates that the nanocomposite performed as an ionic exchanger that created complex formation. Indeed, in the ion exchange mechanism, losing H^+ ions from acid groups can cause Pb ions adsorption. In the ion exchange mechanism, H^+ ions could be easily released using fumaric acid groups and then, lead to ions adsorbing.

3.4. Isotherm and kinetic studies

The Pb adsorption isotherm by the maleate/PAN nanocomposite is shown in Table 3. The isotherm modeling is the most important parameter for design of adsorption systems, which donates a relationship between the adsorption capacity and adsorbent concentration. Langmuir isotherm is defined by single-layer adsorption and on the other hand, Freundlich isotherm is based on multi-layer adsorption of adsorbate. In addition, D-R isotherm applies to present adsorption mechanism with Gaussian energy distribution onto surface adsorbent. According to Table 3, the regression coefficients of Langmuir isotherm were closer to the unity for the adsorption results within the studied concentration range with $R^2 = 0.99$, compared with Freundlich and D-R isotherm with $R^2 = 0.97$ and 0.83, respectively. The results were well congruent with previous data.

The kinetic models of Pb adsorption by the maleate/PAN nanocomposite are illustrated in Fig. 5. Furthermore, the results of kinetic Pb adsorption are shown in Table 3. Indeed,

application of pseudo-first-order and pseudo-second-order models at different concentrations of the lead was studied. In the pseudo-first-order graph, the $\log(q_e - q_t)$ vs. t was plotted to determine the K_1 value and R^2 coefficient. In order to obtain K and q_e in the pseudo-second-order model, the slope and y-intercept of t/q_t vs. t plot were used. Comparison of the R^2 value in the kinetic models shows concordance of the adsorption by the pseudo-second-order kinetics. The results were in agreement with the other studies [22,23].

Furthermore, the results of kinetic Pb adsorption are shown in Table 3. Application of pseudo-first-order and pseudo-second-order models at different concentrations of the lead was studied. In the pseudo-first-order graph, the $\log (q_e - q_t)$ vs. t was plotted to determine the K_1 value and R^2 coefficient. In order to obtain K and q_e in the pseudo-second-order model, the slope and y-intercept of t/q_t vs. t plot were used. Comparison of the R^2 value in the kinetic models shows concordance of the adsorption by the pseudo-second-order kinetic model.

3.5. Comparison of maleate/PAN nanocomposite with other adsorbents

The maleate/PAN nanocomposite synthesized due to its high surface-to-volume ratio which has a better adsorption capacity compared with other synthesized adsorbents presented in Table 4. This result related to the homogeneous distribution of the activated sites on the nanocomposite nanofibers. This study found that the q_{max} is 349.15 mg/g compared with other studies in Table 5. This agrees that maleate/PAN nanocomposite has better performance in case of Pb adsorption from contaminated water.

4. Conclusion

The maleate/PAN nanocomposite was successfully synthesized by electrospinning way followed by coating method and then the electrospun maleate/PAN nanocomposite was characterized for adsorbing lead ions. Based on FESEM graph, the maleate nanoparticles were coated on the PAN nanofibers surface. For optimizing the parameters (Pb concentration, nanocomposite dosage, pH, and contact time), RSM technique was applied. As a result of the RSM optimization, the optimum condition of Pb concentration, maleate/PAN nanocomposite dosage, pH, and contact time were 25 mg/L, 1.85 g/L, 6, and 60 min, respectively, where 98.5% of lead removal was achieved. Based on the isotherm and kinetics modeling, Langmuir isotherm and pseudo-second-order kinetics provided a better fit than other models.

Table 3
Isotherm and kinetic parameters of Pb adsorption onto maleate/PAN nanocomposite

Langmuir	K_L	q_{max}		R^2		$R^2 = 0.96$
	0.021	349.15		0.99	Pseudo-first-order	$K_1 = 0.0269$
Freundlich	K_f	n		R^2		$q_e = 12.10$
	9.98	1.14		0.97		$R^2 = 0.99$
Dubinin–Radushkevich	$q_{m,D\text{-}R}$	β	E	R^2	Pseudo-second-order	$K_2 = 0.252$
	183.29	0.01	11.2	0.83		$q_e = 158.73$

Table 4
Comparing the maleate/PAN nanocomposite with other nanocomposites for lead adsorption

Adsorbents	q_{max} (mg/g)	pH	Contact time (min)	Temperature (°C)	Reference
Magnetic nanocomposite Fe_3O_4/CNT	21.55	3	40	30	[24]
Carboxylate-rich palygorskite	160.2	7	30	25	[4]
Zeolite Y/faujasite nanocomposite	83.26	5.5	40	25	[25]
Sodium aluminum silicate hydrate/ analcime nanocomposite	58.86	5.5	40	25	[25]
Maleate/PAN nanocomposite	349.15	6	60	25	Present study
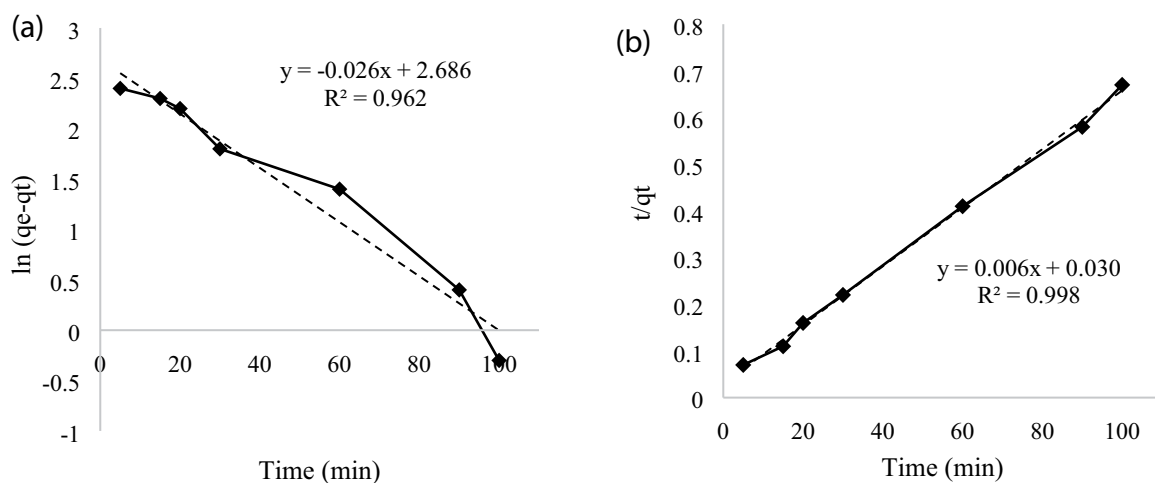
Fig. 5. Kinetic models for Pb adsorption by maleate/PAN nanocomposite. (a) Pseudo-first-order and (b) pseudo-second-order kinetics.

References

[1] N.H. Abdullah, K. Shameli, E.C. Abdullah, L.C. Abdullah, Solid matrices for fabrication of magnetic iron oxide nanocomposites: synthesis, properties, and application for the adsorption of heavy metal ions and dyes, Compos. Part B-Eng., 162 (2019) 538–568.

[2] T.A. Saleh, A. Islam, Synthesis of polyamide grafted carbon microspheres for removal of rhodamine B dye and heavy metals, J. Environ. Chem. Eng., 6 (2018) 5361–5368.

[3] M. Bahrami, M.J. Amiri, F. Bagheri, Optimization of the lead removal from aqueous solution using two starch based adsorbents: design of experiments using response surface methodology (RSM), J. Environ. Chem. Eng., 7 (2019) 102–793.

[4] J. Chen, W. Luo, A. Guo, T. Luo, C. Lin, H. Li, L. Jing, Preparation of a novel carboxylate-rich palygorskite as an adsorbent for Ce^{3+} from aqueous solution, J. Colloid Interface Sci., 512 (2018) 657–664.

[5] G. Moradi, F. Dabirian, P. Mohammadi, L. Rajabi, M. Babaei, N. Shiri, Electrospun fumarate ferroxane/polyacrylonitrile nanocomposite nanofibers adsorbent for lead removal from aqueous solution: characterization and process optimization by response surface methodology, Chem. Eng. Res. Des., 129 (2018) 182–196.

[6] L. Ge, W. Wang, Z. Peng, F. Tan, X. Wang, J. Chen, X. Qiao, Facile fabrication of Fe@MgO magnetic nanocomposites for efficient removal of heavy metal ion and dye from water, Powder Technol., 326 (2018) 393–401.

[7] T.A. Saleh, Mercury sorption by silica/carbon nanotubes and silica/activated carbon: a comparison study, J. Water Supply Res. Technol., 64 (2015) 892–903.

[8] B. Hayati, A. Maleki, F. Najafi, F. Gharibi, G. McKay, V.K. Gupta, S. Harikaranahalli Puttaiah, N. Marzban, Heavy metal adsorption using PAMAM/CNT nanocomposite from aqueous solution in batch and continuous fixed bed systems, Chem. Eng. J., 346 (2018) 258–270.

[9] M. Khazaei, S. Nasseri, M.R. Ganjali, M. Khoobi, R. Nabizadeh, A.H. Mahvi, S. Nazmara, Response surface modeling of lead(II) removal by graphene oxide-Fe_3O_4 nanocomposite using central composite design, J. Environ. Health Sci. Eng., 14 (2016) 2.

[10] T.A. Saleh, Nanocomposite of carbon nanotubes/silica nanoparticles and their use for adsorption of Pb(II): from surface properties to sorption mechanism, Desal. Water Treat. 57 (2016) 10730–10744.

[11] H. Luo, W.W. Law, Y. Wu, W. Zhu, E.H. Yang, Hydrothermal synthesis of needle-like nanocrystalline zeolites from metakaolin and their applications for efficient removal of organic pollutants and heavy metals, Microporous Mesoporous Mater., 272 (2018) 8–15.

[12] A. Maleki, Z. Hajizadeh, V. Sharifi, Z. Emdadi, A green, porous and eco-friendly magnetic geopolymer adsorbent for heavy metals removal from aqueous solutions, J. Cleaner Prod., 215 (2019) 1233–1245.

[13] D. Nandi, I. Saha, S.S. Ray, A. Maity, Development of a reduced-graphene-oxide based superparamagnetic nanocomposite for the removal of nickel(II) from an aqueous medium via a

fluorescence sensor platform, J. Colloid Interface Sci., 454 (2015) 69–79.

[14] N. Nasseh, B. Barikbin, L. Taghavi, M.A. Nasseri, Adsorption of metronidazole antibiotic using a new magnetic nanocomposite from simulated wastewater (isotherm, kinetic and thermodynamic studies), Compos. Part B-Eng., 159 (2019) 146–156.

[15] X. Wang, Y. Wang, S. He, H. Hou, C. Hao, Ultrasonic-assisted synthesis of superabsorbent hydrogels based on sodium lignosulfonate and their adsorption properties for Ni^{2+}, Ultrason. Sonochem., 40 (2018) 221–229.

[16] M. Neelaveni, P. Santhana Krishnan, R. Ramya, G. Sonia Theres, K. Shanthi, Montmorillonite/graphene oxide nanocomposite as superior adsorbent for the adsorption of Rhodamine B and Nickel ion in binary system, Adv Powder Technol., 18 (2019) 1–12.

[17] A. Ates, E. Altintig, H. Demirel, M. Yilmaz, Comparative study on adsorptive removal of Cu, Pb, Zn heavy metals by modified perlite composites, Desal. Water Treat., 98 (2017) 244–253.

[18] B. Priya, S. Kaith, U. Shanker, B. Gupta, J.K. Bhatia, RSM-CCD optimized In-air synthesis of photocatalytic nanocomposite: application in removal-degradation of toxic brilliant blue, React. Funct. Polym., 131 (2018) 107–122.

[19] A. Eslami, M. Mehralian, Z. Godarzvand Chegini, M. Khashij, Application of nanosilica-based adsorbent for the removal of rhodamine B and methylene blue from aqueous solutions, Desal. Water Treat., 108 (2018) 345–352.

[20] R. Rusmin, B. Sarkar, T. Tsuzuki, N. Kawashima, R. Naidu, Removal of lead from aqueous solution using superparamagnetic palygorskite nanocomposite: material characterization and regeneration studies, Chemosphere, 186 (2017) 1006–1015.

[21] M.M. Sadeghi, A.S. Rad, M. Ardjmand, A. Mirabi, Preparation of magnetic nanocomposite based on polyaniline/Fe_3O_4 towards removal of lead(II) ions from real samples, Synth. Met., 245 (2018) 1–9.

[22] K.M. Seema, B.B. Mamba, J. Njuguna, R.Z. Bakhtizin, A.K. Mishra, Removal of lead(II) from aqueous waste using (CD-PCL-TiO_2) bio-nanocomposites, Int. J. Biol. Macromol., 109 (2018) 136–142.

[23] C. Liu, M. Zhao, S. He, Z. Cao, W. Chen, Fe_3O_4 magnetic nanoparticles as a catalyst of oxone for the removal of a typical amino acid, Desal. Water Treat., 97 (2017) 262–271.

[24] F. Elmi, T. Hosseini, M.S. Taleshi, F. Taleshi, Kinetic and thermodynamic investigation into the lead adsorption process from wastewater through magnetic nanocomposite Fe_3O_4/CNT, Nanotechnol. Environ. Eng., 2 (2017) 13.

[25] EA. Abdelrahman, A. Alharbi, A. Subaihi, A.M. Hameed, M.A. Almutairi, F.K. Algethami, H.M. Youssef, Facile fabrication of novel analcime/sodium aluminum silicate hydrate and zeolite Y/faujasite mesoporous nanocomposites for efficient removal of Cu(II) and Pb(II) ions from aqueous media, J. Mater. Res, Technol., 9 (2020) 7900–7914.